JOURNAL OF THERMOPHYSICS AND HEAT TRANSFER
Vol. 20, No. 3, July–September 2006

Material Dependence of Plasma Radiation Produced by a Capillary Discharge

Malay Das,* Stefan T. Thynell,† Jianquan Li,* and Thomas A. Litzinger†
Pennsylvania State University, University Park, Pennsylvania 16802

An experimental investigation has been conducted on the radiative heat transfer from an electrothermal–chemical plasma jet. The plasma jet was initiated by a 3.6-mg thin metallic wire within a 3.2 mm diameter and 26 mm long capillary. During the discharge of the 0.6 kJ of electrical energy, the plasma evolved from the capillary into an ambient air environment as an underexpanded supersonic jet that interacted with a stagnation plate. The effect of capillary and trigger wire materials on the radiative heat transfer between the plasma jet and stagnation plate was investigated. Experiments were conducted with nine different combinations of capillary and wire materials. Various diagnostic techniques were used, including heat flux and pressure gauges mounted on the stagnation plate, as well as a high-resolution charge-coupled device camera for flow visualization. A fused-silica window, placed about 1 mm above the gauges, ensured that only the radiative heat flux transmitted by the window was deduced. The results show that appreciable differences are present among the capillary and wire combinations, with a polycarbonate capillary and copper wire yielding the largest energy deposition in the substrate, whereas Teflon®–nickel yielded the lowest.

Nomenclature

c_p	=	specific heat, J/kg · K
I_{av}	=	mean value of current, A
I_{pot}	=	ionization potential, eV
k	=	conductivity, W/m · K
$q_{\max}$	=	peak heat flux, W/m^2
q''	=	heat flux, W/m^2
T	=	temperature, K
$T_{\max}$	=	maximum temperature, K
T_{ref}	=	ambient temperature, K
t	=	time, s
V_{av}	=	mean value of voltage
$V(t)$	=	voltage at time t, V
α	=	thermal diffusivity, m^2/s
β	=	temperature coefficient of resistivity, 1/K
ρ	=	density, kg/m^3
σ	=	standard deviation

Introduction

RECENTLY, electrothermal–chemical (ETC) ignition of solid propellants, showing several advantages over the conventional chemical ignition, has received considerable attention.[1–9] ETC ignition system uses a high-temperature, high-pressure plasma jet involving several modes of energy transport. These include convection, radiation, and vapor condensation. Characterization of different energy transport mechanisms and identification of their relative roles in propellant ignition and combustion will considerably add to the present understanding of ETC ignition system development. Available studies, however, provide only a limited amount of information, emphasizing the necessity of further investigations in several areas. The role of radiative heat transfer constitutes one of these unresolved areas.

Radiative heat transfer is regarded as an important mode of energy transport during ETC ignition. The high-temperature plasma contains electrons, atoms, and low-molecular-weight species from capillary and electrode ablation, thus providing a substantial source of radiative heat flux in the UV-visible wavelength range.[10] Beyer and Pesce-Rodriguez[11] exposed research propellants to the effects of plasma radiation alone. The plasma was confined within a polycarbonate tube, resulting in a spectral UV cutoff near 350 nm. Mass loss, Fourier-transform infrared spectrometry, and optical microscopy were used to examine recovered samples and captured evolved gases. Schroeder et al.[12] used the same apparatus and scanning electron microscopy to study recovered propellant samples. In these studies, it was clear that the highly transparent graphite-free JA2 responded more strongly to the plasma radiation than samples with much larger absorption coefficients. The pulse length also had a strong impact on the extent of mass loss, with a shorter, more intense pulse having a stronger effect when considering the same energy level.

Wren et al.[13] modeled and numerically simulated the effect of radiative contribution in ETC ignition. Their model investigated the combustion of 27.06 g of granular JA2 propellant within a 129-cm^3 closed chamber ignited by a 29-kJ ETC plasma, generated within a 0.32-cm-radius polyethylene capillary. This model utilized a one-dimensional plasma flow solver for plasma characterization, experimental data for electrical current history, and a previously benchmarked three-dimensional, multiphase Navier–Stokes solver with Lagrangian representation of propellant grains. Lagrangian representation allowed each propellant particle to attain different bulk temperature, diameter, burning rate, and thermophysical and chemical properties. Whereas the convective flux dictated the ignition, they concluded that radiant energy modifies grain bulk temperature and thermochemical properties, resulting in a substantial increase in the burning rate.

Taylor,[14–18] on the other hand, estimated the radiative heat flux in plasma–propellant interactions using time-resolved UV/visible spectroscopy. Measurements covered a wavelength range from 369 to 1027 nm, and spectra were acquired at a time resolution of about 50 μs. Experiments were conducted in two different configurations. Aluminum or copper wires of 0.5 mm diameter were used as plasma initiators. In the first case, the exploding wire was placed coaxially with an open-ended propellant cylinder. The second test case was conducted in a 400-cm^3 closed chamber by placing the propellant at one endplate and a capillary plasma generator at the opposite endplate. A conventional ignition system using a puffer bag was also tested in the second configuration. When a translucent propellant was used, it was concluded that the damage sustained in the propellant's internal grain structure was not attributed to the radiative heat

Received 1 June 2005; revision received 22 August 2005; accepted for publication 23 August 2005.

*Research Assistant, Department of Mechanical and Nuclear Engineering. Member AIAA.

†Professor, Department of Mechanical and Nuclear Engineering. Senior Member AIAA.

flux. The type of material used for the plasma initiation wire played an important role in the damage of the propellant's grain structure. Metal vapor condensation was concluded to be the primary source of energy transport. Radiative and total heat flux measurements were performed by Ryan et al.[19] using a commercially available gauge. Although electrical noise was apparent at close distances (47 mm) and prevented acquisition of data while the electrical discharge occurred, the deduced heat flux levels were quite large.

The role of radiant energy transfer in ETC ignition, however, is difficult to ascertain without an assessment of the roles of capillary and wire materials, as well as the role of the radiative properties of propellants. Information about average heat flux rates to plasma-exposed surfaces was deduced by Williams and White.[20] They allowed plasma impingement on a black carbon-coated thin copper plate. The temperature history on the back side of the plate was captured using an unfiltered infrared camera. An inverse analysis was utilized to deduce average heat flux rates from the temperature data. This work served as a refinement of the earlier effort by White et al.,[21] in which thermocouples were used on the back side of the copper plate. Infrared photography was utilized rather than thermocouples because the electrical noise, likely caused by rapidly varying electromagnetic fields, was significant for low-voltage thermocouple measurements. Williams and Beyer[22] again utilized the copper plate–thermocouple combination to compare short ($\sim$1 ms) and long pulse ($\sim$7 ms) noncapillary sustained plasma radiation. Restricting convective flux by a polycarbonate window, they deduced much higher average radiant flux for short pulse plasma.

Experimental investigations were supplemented by several numerical efforts of solving mass, momentum, energy, state, and Maxwell's equations. Gruber et al.[23] and Kappen and Bauder[24,25] developed a model of spectral radiative heat transfer from high-temperature and high-pressure plasmas. Based on the assumption of local thermodynamic equilibrium (LTE), that is, translational, rotational, and vibrational temperatures are equal, complete tables of radiation characteristics for ETC gun interior ballistics was generated for JA2 propellant in 300–45,000 K temperature range. Following the assumptions of LTE and neglecting scattering, the radiative transport equation (RTE) was solved numerically by the method of partial characteristics. Radial variation of temperature, radiative intensity, and heat flux were reported for a closed-chamber configuration. Results confirmed the dominance of radiant flux in the UV range over visible infrared (IR) in the high-temperature zone. This dominance, however, gradually diminishes with the fall of temperature and finally stabilizes with equal heat fluxes for the UV and the visible-IR zones.

The limited information on the transient variation of the radiant heat flux prompted Das et al.[10] to design and manufacture a heat flux gauge comprising a thin film of platinum on polyimide. A 26-mm-long and 3.2-mm-diam polyethylene capillary was used with 0.08-mm-diam copper trigger wire. The plasma discharged into ambient air through a 3.2-mm-diam and 26-mm-long elkonite (30% Cu and 70% W) nozzle. A stagnation plate, equipped with the heat flux gauges, was placed at a distance of 50 or 75 mm from the nozzle outlet. Plasma charging voltages were kept at 2.5 (0.6) and 3.0 kV (0.86 kJ). A maximum radiative heat flux of about 14 MW/m^2 was recorded for the 2.5-kV, 50-mm configuration; gauges were destroyed for a charging voltage of 4.0 kV for a nozzle outlet to stagnation plate distance of 50 mm.

The preceding discussion reveals a variety of approaches are utilized to ascertain the radiative characteristics of capillary sustained plasma, which may account for improved ignition of solid propellants. Present research aims to contribute to the understanding of the capillary and wire material dependence of radiative heat flux from an ETC plasma jet. Following a procedure similar to Das et al.,[10] nine different combinations of capillary-wire materials have been investigated. Transient pressure, temperature, and radiant heat flux measurements have been carried out, along with flow visualization.

Experimental Apparatus and Approach

Plasma Generator

The present study uses a pulse-forming network (PFN) circuit for plasma initiation, discussed elsewhere in detail.[10] The PFN comprises two capacitors connected in parallel to yield a total capacitance of 192 μF, a 20-μH inductor, a crowbar diode, an ignitron, and an ignitron-triggering circuit. The capacitors can be charged up to 10 kV to yield a maximum energy storage of 9.6 kJ. For the present experiment, the voltage is kept constant at 2.5 kV generating a 0.6-kJ plasma. The plasma chamber consists of a capillary, a fine metallic wire, electrodes, and other nonconducting housing hardware. The capillary has a bore length of 26 mm and a typical diameter of 3.2 mm. Located at each end of the capillary is an electrode made of elkonite (copper–tungsten alloy, 30% Cu and 70% W), which is resistant to material erosion. A fine 3.6-mg wire (50–75 μm diameter) that runs through the capillary and connects the electrodes serves as the discharge initiator. After being formed immediately on triggering of the ignitron, the plasma flows through a nozzle that has dimensions of 3.2 mm (orifice diameter) and 26 mm (length) into the ambient open-air environment. The nozzle is designed to have this length for accommodating the relatively large dimensions of the plasma chamber.

Once evolved from the nozzle, the plasma impinges on a stagnation plate. Heat flux and pressure gauges are placed on the stagnation plate as shown in Fig. 1. Heat flux gauges are covered with two fused silica windows (S1-UV, ESCO Products): one sacrificial 1.59 mm

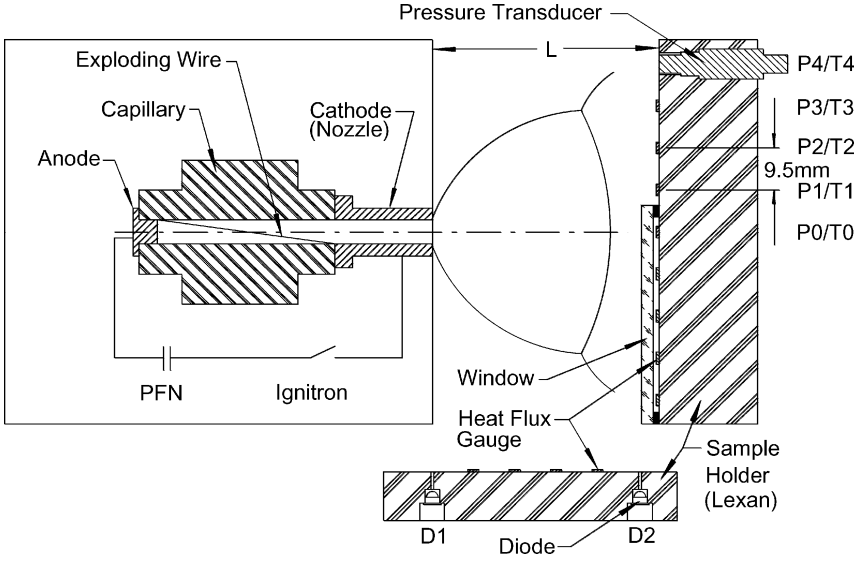

Fig. 1 Pressure transducer, heat flux gauge, and diode locations with respect to plasma emergence from capillary.

thick and a second 4.76 mm thick. The fused silica windows are in contact with each other. The window is needed for two reasons. First, the goal is to allow a determination of the radiative heat flux as opposed to the total heat flux (radiative, convective, and heat release from recombination reactions). The use of fused silica windows allows the former but prevents the latter two energy exchange mechanisms. Second, some ionic species or charged particles arrive at the plasma–solid interface and tend to produce significant electrical noise. The fused silica window transmits radiation within 170–2500 nm wavelength range and reflects about 12% of the radiant heat flux.[10] The details of gauge locations, pressure gauge specifications, and window effects are discussed elsewhere.[10]

Side-view images of the plasma were taken using a Cordin Model 222-B charge-coupled device (CCD) camera with a Pentax 6×7 mount 105-mm lens. It consists of 8 CCDs and is capable of acquiring 16 images, each with a resolution of 1300 by 1030 pixels, a 10-bit dynamic range, and exposure gates down to 10 ns. The first and last 8 images can be acquired at a speed of up to 10^8 pictures per second, but these two sets of 8 images are interrupted by a delay of several microseconds for transfer of the charge. Neutral density filters and extension tubes were used as per requirements.

To estimate the plasma composition, capillary, nozzle, and the electrode masses were measured before and after each experiment. For this purpose, a Denver Instrument XE50 spring balance was used. The mass balance has a digital display and a minimum measurement capability of 0.0001 g.

Heat Flux Gauge Design

Thin-film platinum (80 nm) sputtered over polyimide (50 μm) was used for deducing the transient variation of the radiative heat flux. A National Semiconductor's LM 134 constant current source, set at 3 mA, powered by low-noise 9-V battery, is connected to the platinum gauge via 500-nm sputtered copper leads. The gauge was attached to a SS304 substrate through a transfer tape. The operating principle and the design and manufacturing procedure of the gauge, as well as the characteristics of the constant current source, have been discussed elsewhere in detail.[10]

Data Reduction

A standard inverse approach was employed to estimate the transient, absorbed radiative heat flux variation from the measured time-dependent voltage data. The model assumes that conductive transfer in the polyimide film is one dimensional, that a perfect thermal contact is made between the platinum film and the polyimide substrate, and that thermophysical properties are constant. For $0 < x < \infty$ and $0 < t < t_f$, the inverse problem is governed by

$$k\frac{\partial^2 T}{\partial x^2} = pc\frac{\partial T}{\partial t} \tag{1}$$

$$-k\frac{\partial T}{\partial x} = q''(t) \qquad \text{at} \qquad x = 0 \tag{2a}$$

$$T = T_{\text{ref}} \qquad \text{at} \qquad x \to \infty \tag{2b}$$

$$T = T_{\text{ref}} \qquad \text{at} \qquad t = 0 \tag{2c}$$

where $q''(t)$ is the unknown, absorbed radiative heat flux. Based on the conjugate-gradient approach described in detail by Ozisik,[26] a numerical procedure was developed. The inverse data reduction technique was applied to the measured surface temperature to determine the absorbed, radiative heat flux. The model used a thermal conductivity $k = 0.25$ W/m K, which is the normal conductivity obtained by Kurabayashi et al.,[27] $\rho = 1{,}420$ kg/m^3, and $c_p = 1{,}040$ J/kg K of the polyimide substrate. Justification for using the one-dimensional model and uncertainties related to the data reduction procedure has been discussed.[10]

The temperature coefficient of the electrical resistivity of platinum $\beta = 0.002$/K was assumed to be linear over the temperature range from 20 to 220°C, and it was deduced from measurements using a standard convection oven. This value is about 50% lower than the bulk value (0.00389/K). For the manufactured film thickness of 80 nm, the incident radiant energy is either absorbed or reflected by the platinum film; the transmissivity is practically zero. The theoretical spectral absorptivity of platinum can be roughly estimated using bulk properties.[28,29] The diffuse or normal spectral absorptivity is about 0.75 at 200 nm, decreases to 0.4 at 400 nm, and is about 0.32 at 600 nm. The platinum film appears slightly dark to the naked eye.

Capillary and Wire Materials

Three different materials are used for the capillaries: high-density polyethylene (PE), polycarbonate [popularly known as Lexan (LE)] and polytetrafluroethylene [Teflon® (TE)]. These materials were acquired from McMaster–Carr (available online at http://www.mcmaster.com [cited 5 January 2005]) and machined to appropriate dimensions using standard techniques. The molecular structures of monomer units of these compounds are shown in Fig. 2. The effects of three different wire materials were examined: copper (Cu), nickel (Ni) and aluminum (Al). The high pressures and temperatures within the capillary are generally believed to completely vaporize the initiator wire. However, the extent of ablation of the capillary is strongly dependent on its physicochemical properties shown in Table 1. There are numerous studies available in the literature that have attempted to elucidate the thermal decomposition

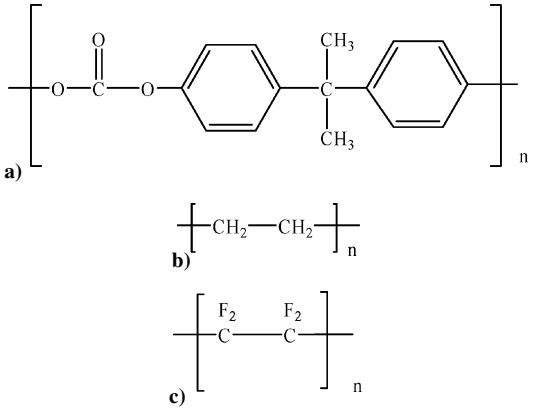

Fig. 2 Molecular structures of repeated monomer units in a) LE, b) PE, and c) TE.

Table 1 Relevant physicochemical properties of capillary and wire materials

Material	ρ, kg/m^3	c_p, kJ/kg · K	k, W/m · K	T_{melt}, K	T_{dec}, K	T_{boil}, K	h_{fg}, kJ/kg	I_{pot}, eV
PE	950	1900	0.49	390	670–800	——	——	——
LE	1200	1200	0.20	——	670–800	——	——	——
TE	2200	1000	0.25	617	770–920	——	——	——
Al	2700	900	237	933	——	2740	10800	5.99
Cu	8960	385	401	1356	——	2840	4796	7.73
Ni	8900	444	91	1726	——	3005	6378	7.63
H	——	——	——	——	——	——	——	13.59
C	——	——	——	——	——	——	——	11.26
N	——	——	——	——	——	——	——	14.53
O	——	——	——	——	——	——	——	13.61
F	——	——	——	——	——	——	——	17.40

characteristics of these capillary materials under low heating rates, with and without the use of catalyst.

The thermal stability of TE is largely derived from the strong C–F bond of 507 kJ/mol, compared to typical values of 415 kJ/mol for C–H and 348 kJ/mol for C–C bonds.[30,31] When thermogravimetric techniques with heating rates at 25 K/min are used, melting of TE is observed around 617 K, noticeable decomposition begins to occur around 770 K, and complete decomposition is observed near 920 K in atmospheric conditions. Decomposition products include C_2F_4, C_3F_6, and C_4F_8 (Ref. 32). Ceramics, such as Si and $CaSi_2$, produce exothermic decomposition, whereas Fe and FeSi yield endothermic decomposition. Fe has nearly no effect on the kinetic rates of decomposition. Additionally, it should be noted that TE can be used as an oxidizing agent, although the strong C–F bond is strong.[33] Flares and igniters often utilize a metal/PTFE/Viton combination to produce combustion products of very high temperatures.[34] Polytetrafluroethylene (PTFE) is also considered for use in pulsed plasma thrusters.[35]

PE is a rather soft material compared to TE. As a result, the high pressures within the PE capillary are likely to cause a volumetric expansion. Thermogravimetric techniques, with a heating rate of 25 K/min, reveal melting near 388 K, onset of decomposition around 670K, and complete decomposition near 800 K (Ref. 36). The gaseous products contain a large fraction of C3 compounds, whereas the residue comprises largely aromatics.[37,38]

Polycarbonates are commonly used in rewritable compact discs, eye glasses, medical parts, aircraft, and appliances due to their toughness, transparency, and good mechanical and thermal stability. When thermogravimetric techniques at 10 K/min are used, onset of decomposition occurs around 670 K and is complete near 800 K (Ref. 39). Gaseous products evolved at temperatures from 770 to 820 K contain a wide variety of compounds, suggesting many different pyrolysis processes.[40]

The PE and LE compounds have also been subjected to high heating rates and temperatures due to an arc jet environment.[41] Temperatures of 5100 K were lower than those deduced from capillary discharges of 10,000 to 50,000 K (Refs. 42 and 43). As such, radiative contributions from ions, ion recombination reactions, and atomic species are likely to be larger contributors to radiative heat transfer from capillary discharges compared to the arc jet environment. When spectrographic techniques covering a wavelength range from 250 to 870 nm are used, species identified in the arc jet as having significant contributions include the C_2 swan band, CN red and violet bands, CO Asundi band (see Ref. 44), and CH, as well as chemiluminescence from CO+O (Ref. 41). Hence, reactions between pyrolysis products from the ablated plastics and ambient air will produce species that contribute significantly to the radiative heat transfer in capillary discharges as well.

Discussion of Results

The use of the basic resistive-inductive-capacitive (RLC)–electrical circuit yields highly repeatable data from the two current transducers, pressure transducers, and heat flux gauges. Deviations in these measured parameters are typically only a few percent between the experiments, resulting in a small uncertainty. A larger uncertainty is obtained for the deduced radiative heat flux, which is inherent in the use of inverse techniques. The uncertainties are indicated by error bars at $\pm 2\sigma$, where σ is the standard deviation based on three independent estimations. Electrical noise is most pronounced during the first 20 μs, or when the plasma is being formed. Some additional noise occurs during voltage reversals, which occur because the electrical circuit is slightly underdamped. A charging voltage of 2.5 kV, trigger wire mass of 3.6 mg, and distance between capillary exit nozzle and stagnation plate of 50 mm were kept constant; all experiments were conducted in an open-air environment. The discussion of results is first focused on differences in the voltage and current traces for the various capillary and wire combinations.

Figure 3 shows the acquired voltage and current in the capillary. The corresponding data on ablated mass from the various components, as well as the average voltages and currents, are listed in Table 2. Here, the elkonite nozzle, which is a tube of 25 mm in length and 3.2 mm in diameter, is also the negative electrode. Several interesting features are observed. First, the trigger wire has the largest influence on the variation on the voltage drop across electrodes attached to the capillary and the current flow within the capillary. The Al wire, with its relatively low melting and boiling points, as well as a low ionization potential, provides the smoothest transition from current flow in the wire to current flow within the plasma. This smooth transition for Al yields the lowest peak voltages and smoothest variations in the current from $t = 0$ to $t = 50$ μs. For $t > 50$ μs, the current flow varies smoothly throughout the event, and because the charging energy level is kept constant, peak values of current are slightly lower than those obtained from using either the Cu or Ni wires. The Ni produces the largest delay in current flow, from about 10 to 20 μs, probably due in large part its higher melting and boiling points, and about its twice molecular weight compared to Al. That is, fewer Ni atoms are available to become charge carrier compared to Al. Another important property is surface tension

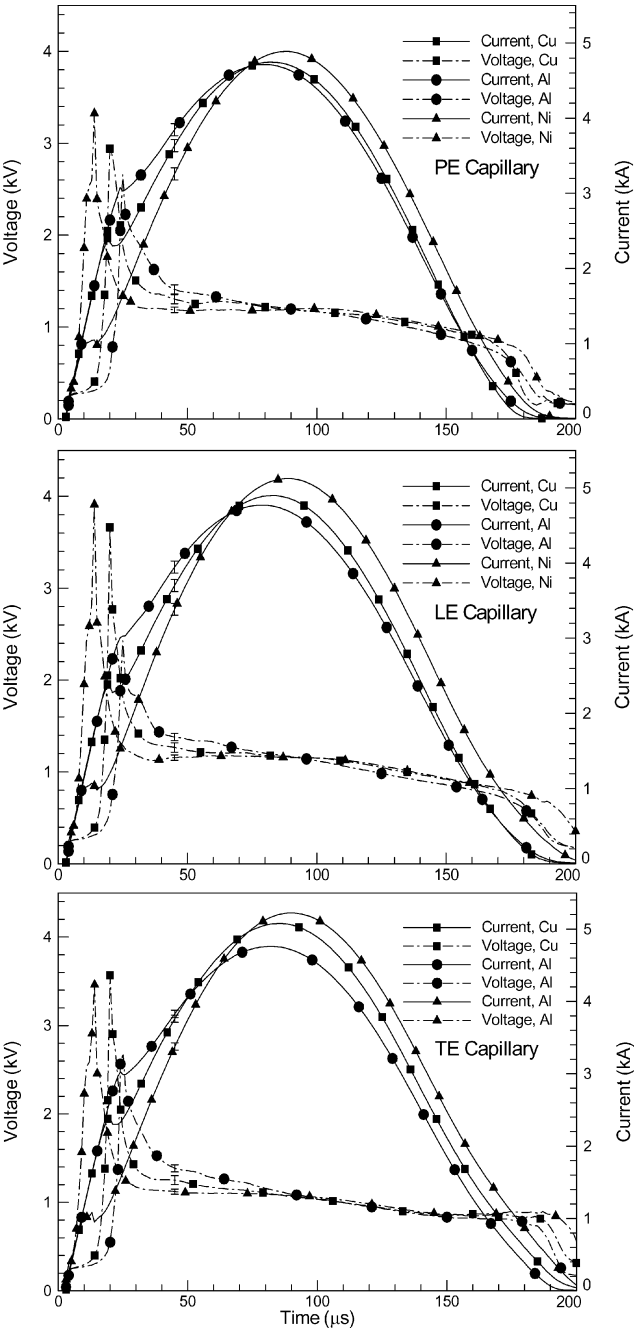

Fig. 3 Voltage and current within capillary during discharge of 0.6 kJ of electrical energy (2.5 kV) for different capillary and initiator wire materials.

Table 2 Mass ablated as well as average voltage and current for different capillary and wire material combinations

Material	Ablated mass, mg	Capillary, %	Nozzle, %	Electrode, %	Wire, %	V_{ave}, kV	I_{ave}, kA
PE+Cu	6.93	26.44	15.53	6.10	51.93	1.007	2.609
PE+Al	6.57	17.26	20.66	7.25	54.13	0.984	2.649
PE+Ni	6.19	26.39	11.68	3.76	58.17	1.070	2.632
LE+Cu	6.95	40.26	5.42	2.55	51.77	1.000	2.719
LE+Al	7.15	32.60	8.43	9.03	50.33	0.961	2.715
LE+Ni	6.52	38.34	2.04	4.41	55.21	1.076	2.832
TE+Cu	10.83	56.31	7.89	2.57	33.23	0.990	2.922
TE+Al	10.20	54.24	6.44	4.03	35.29	0.970	2.778
TE+Ni	11.23	57.86	8.31	1.78	32.05	1.054	2.949

of the molten trigger metal, which forms small droplets during the transition to a gaseous state within the capillary to form a plasma. The initiation transients of plasma formation have been discussed elsewhere.[16,45–47]

Second, the use of the TE capillary yields the highest values of the peak currents and, thus, generally the lowest average voltages. This may suggest that the total number of charge carries within the plasma is the largest for TE capillary. Such a finding would be quite surprising because TE is the most thermally stable material of the three capillaries. From the results shown in Table 2, approximately 0.68 mmole of TE is ablated (considering only the monomer structure of Fig. 2), whereas 0.89 and 1.41 mmole are ablated from the LE and PE capillaries, respectively. Hence, a mechanism of extensive C and F ionization can possibly explain the efficient charge transport through TE capillary.

Third, it is difficult to ascertain when the plasma transitions from one largely containing atoms and ions from the trigger wire to another containing largely atoms and ions from the trigger wire and ablated capillary. Because the decomposition temperatures of the capillary materials do not vary significantly and that pressures and temperatures rapidly increase to extremely high levels, the plasma is believed to contain species from the capillary very early in the event. For the case involving TE, this is most likely in the time interval from 20 to 30 μs into the event.

Figure 4 shows the transient temperature, radiant heat flux, and stagnation pressure variation on the stagnation plate at the exit port centerline for the PE capillary and Cu, Al, and Ni trigger wires. Also here, several distinct differences are observed. The use of the Al wire, with its smoothly varying current, produces the largest peak radiant heat flux. The radiant heating begins around 40 μs into the event, indicating that plasma emergence is rapid. Peak radiant heat fluxes are obtained before arrival of the precursor shock, and they generally coincide with the peak of the current flow. Cases with Cu and Ni wires suggest a slight change or increase (second rise) when peak stagnation pressures are achieved. It is not clear if this effect is a chemically induced effect caused by reactions between Ni and surrounding air, or differences in the radiative properties between Al, Cu, and Ni. The secondary increased radiative heat flux for Cu and Ni is not caused by the arrival of particles (from wire or nozzle) because the quartz window remains quite clear after one firing. However, inspection of atomic line data reveals that neutral and singly ionized Al has relatively few lines produced by electronic transitions covering wavelengths from 200 to approximately 700 nm, whereas Cu and Ni have a much larger number of lines.[48] Any further assessment regarding spectral emission characteristics requires additional experiments. The compressible flow produces strong pressure oscillations that appear quite insensitive to the type of trigger wire material used. The large peak radiant heat flux from the case with Al wire may only partially contribute to a reduced plasma temperature and thus produces the lowest peak pressure; the reduction is much more likely due to a lower plasma density. The differences in peak temperatures between the three wires remain quite small or about 7 K, suggesting that differences in the integrated absorbed heat flux (amount of energy absorbed) is also quite small.

Figures 5 and 6 show the radiative heat flux, temperature, and stagnation pressure for LE and TE capillaries, respectively. The trends

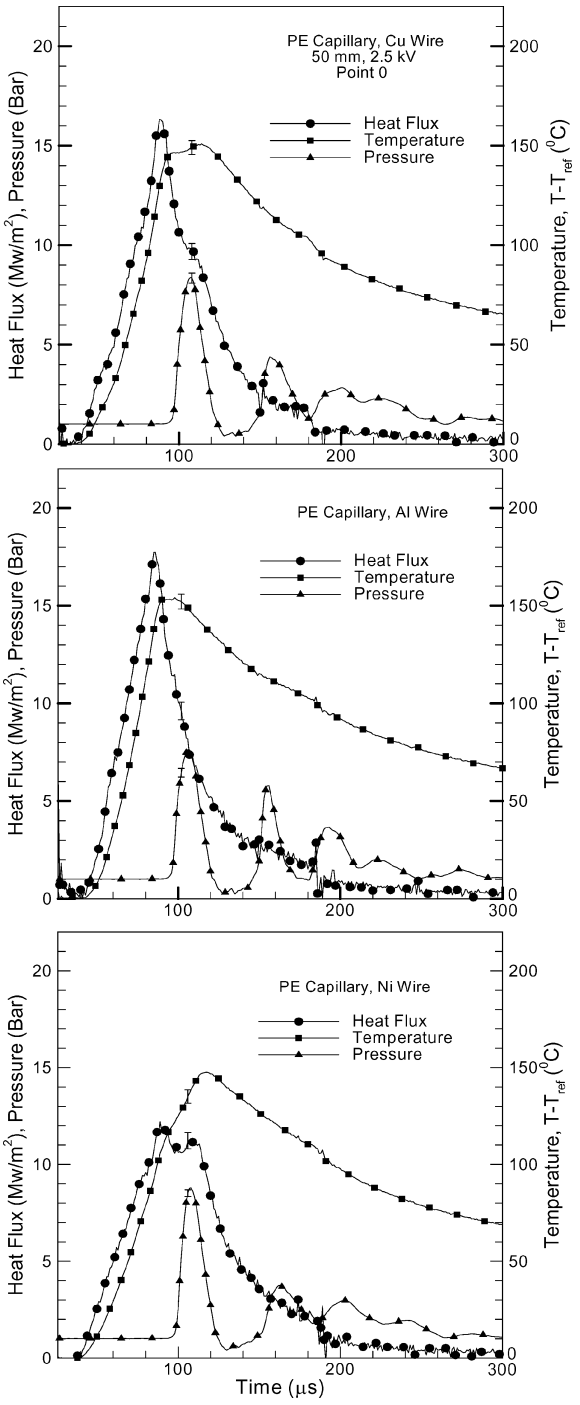

Fig. 4 Transient variation of pressure, temperature, and heat flux at stagnation location for polyethylene capillary and different wire materials with 2.5-kV charging voltage 50 mm from plasma exit port to stagnation plate.

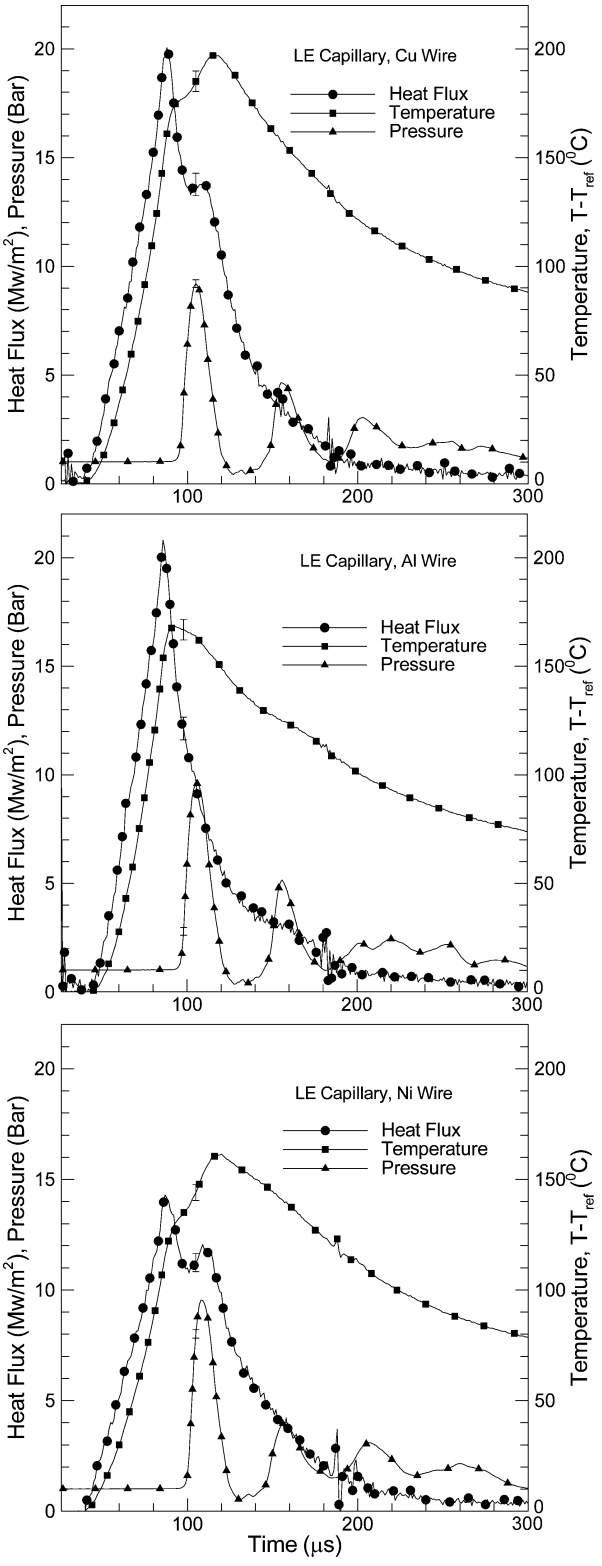

Fig. 5 Transient variation of pressure, temperature, and heat flux at stagnation location for LE capillary and Ni wire with 2.5-kV charging voltage 50 mm from plasma exit port to stagnation plate.

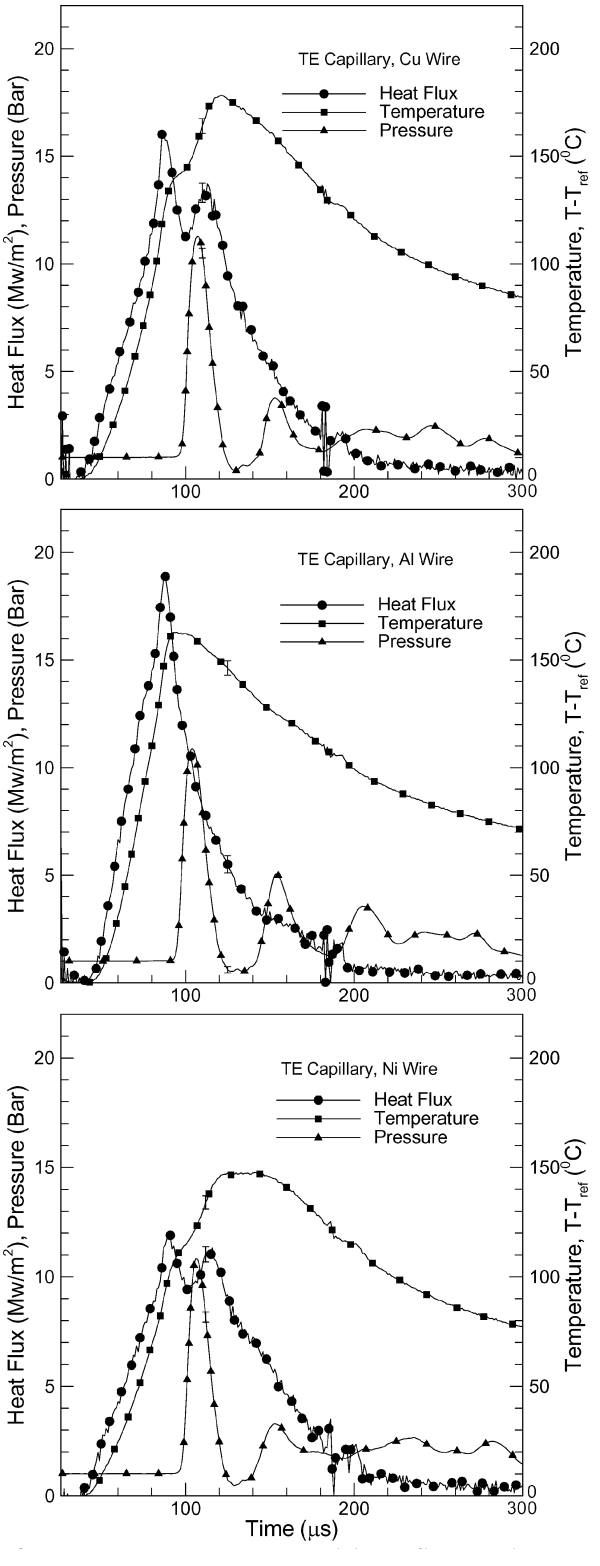

Fig. 6 Transient variation of pressure, temperature, and heat flux at stagnation location for TE capillary and different wire materials with 2.5-kV charging voltage 50 mm from plasma exit port to stagnation plate.

observed in Fig. 4 remain, although the magnitudes are considerably different. First, the LE–Cu combination produces peak temperatures of nearly 200°C of the heat flux gauge, compared to the lowest of about 150°C for the PE–Ni combination; hence, the absorbed energy flux is significantly higher for the LE–Cu combination, which then most likely would produce the highest probability of transition from ignition to combustion of an energetic material. The PE capillary produces generally the lowest temperatures. The use of the Ni trigger wire yields consistently the lowest radiative heat fluxes. However, the TE capillary consistently yields the largest stagnation pressure, although the fewest number of moles are ablated. To shed some light on these findings, it is instructive to examine CCD images for selected capillary trigger wire combinations.

Figure 7 shows images acquired by the Cordin 222-B CCD camera with the first (top) image 80 μs after triggering and subsequent images separated by 10 μs. Thus, the time interval of the primary and

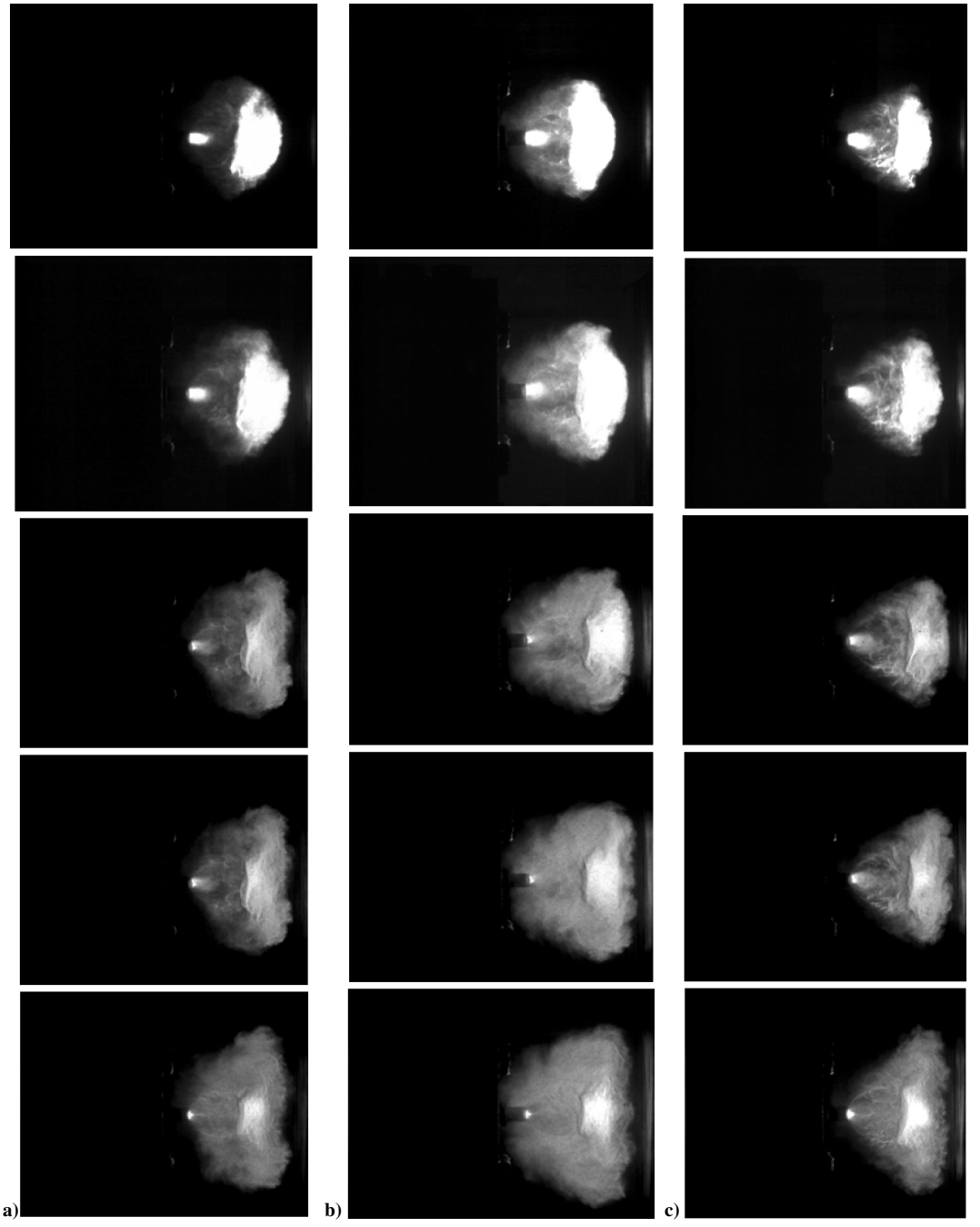

Fig. 7 Side view of plasma for 2.5-kV charging voltage, at 80 (top), 90, 100, 110, 120 μs (bottom) after triggering, for a) PE capillary and Cu wire, b) LE capillary and Al wire, and c) TE capillary and Ni wire.

secondary rises in the heat flux is covered. Images were captured for three different capillary-wire material combinations: PE–Cu, LE–Al, and TE–Ni. Exposure time (20 ns) and aperture (ℓ/11) were kept constant for all of the images authorizing image brightness to be an indication of the plasma temperature.[42] The middle image corresponds to peak pressure and possible arrival of precursor shock, which should be close to jet surface at this time. The images reveal possible highest temperature plasma generation for the LE–Al case, followed by PE–Cu and TE–Ni, respectively. Again a smaller radial expansion of the jet along with a higher mass ablation that produces a larger density may eventually explain higher stagnation pressure of TE capillaries. The lower-density plasma from PE in general produces the lower stagnation pressures. The LE–Al combination produces the largest radial expansion due to very high plasma temperatures and pressures. In addition, the primary and secondary peaks in the emitted radiant flux are observed in the images of Figs. 7a and 7c, whereas Fig. 7b for Al shows a gradual decrease in brightness from top to bottom. General features of the underexpanded supersonic jets have been discussed elsewhere.[6,8,9,49]

To provide information on the profile of the radiative heat flux and temperature, values at four additional gauge locations are provided in Figs. 8 and 9, respectively. The distance between each gauge is 9.53 mm. A total of five gauges are used. Examination of Figs. 8 and 9 reveals that the radiative heat flux decays considerably away from the centerline of the jet for any capillary and wire material combination. The outermost gauge is located 38 mm from the centerline. Comparison with Fig. 7 shows that this gauge is close to the edge of the Mach disk. It is also interesting that the PE–Ni plasma shows the least radial decay, the basis for which is not fully clear. Ni trigger wire clearly plays an important role because the other combinations LE–Ni and TE–Ni also show the lowest radial decay.

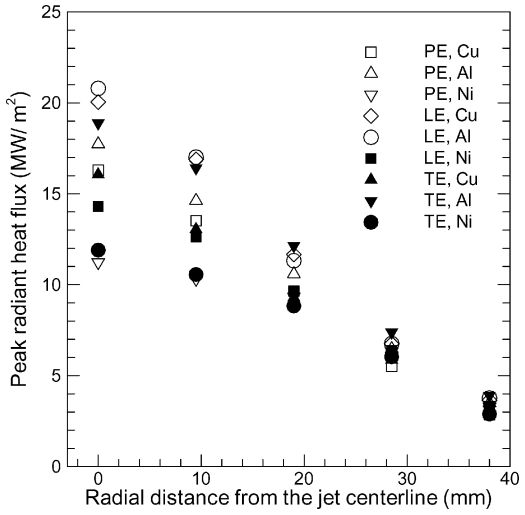

Fig. 8 Variation of peak heat flux with radial distance from centerline for 2.5-kV (0.6-kJ) capillary plasma and distance of 50 mm between plasma port and stagnation plate.

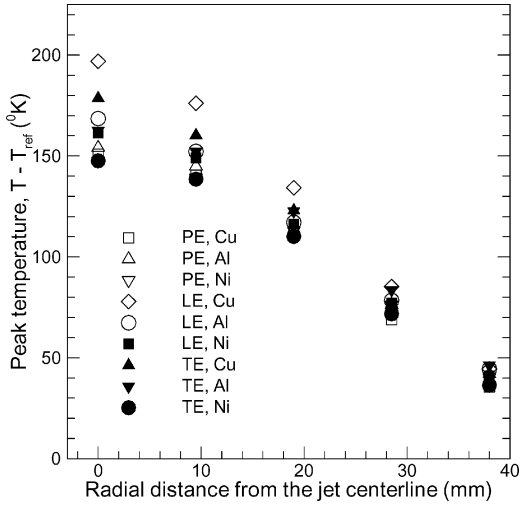

Fig. 9 Variation of peak temperature with radial distance from centerline for 2.5-kV (0.6-kJ) capillary plasma and distance of 50 mm between plasma port and stagnation plate.

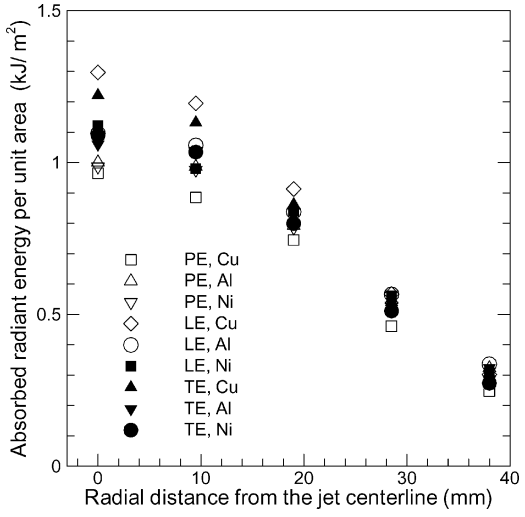

Fig. 10 Variation of absorbed radiant energy per unit area with radial distance from centerline for 2.5-kV (0.6-kJ) capillary plasma and distance of 50 mm between plasma port and stagnation plate.

The temperature rise of a heat flux gauge indicates the cumulative effects of absorption of radiant heat flux at the gauge location. The present results display several cases of multistage temperature rises, along with material dependence of spatial and temporal temperature gradients. The absorbed radiant energy at a location can be determined by numerically integrating the discrete heat flux data over time. Figure 10 presents the radial variation of absorbed radiant energy per unit area. The radiative heat fluxes are integrated over 25–500 μs because the transient flux levels are significant in this period. Closely following the pattern of Fig. 9, the results expectedly shows that the LE–Cu combination produces the largest cumulative absorbed radiative energy flux for the cases considered, followed by TE–Cu.

Conclusions

Capillary and trigger wire material dependence of the radiative heat flux from an electrothermal chemical plasma jet was investigated experimentally. Thin platinum film sputtered on a polyimide substrate was utilized for deducing the transient variation of the absorbed radiative heat flux emitted from the plasma produced by the capillary discharge. Three different capillary materials (PE, LE, and TE) along with three different initiation wire materials (Cu, Al, and Ni) were studied. All of the experiments were conducted in an open-air atmosphere with a constant charging voltage (2.5 kV) and wire mass (3.6 mg). The major findings from this study are as follows.

1) The LE capillary with Al trigger wire generates the smoothest transition to a plasma and the largest peak radiative heat flux, owing in large part to the low melting and boiling temperatures as well as ionization potential of Al.

2) The LE capillary with Cu wire produce a substantially higher absorbed energy flux compared to the other capillary and wire combinations.

3) Depending on the capillary and wire material combinations, radiative heating can be single- or multistaged; the latter possibly involves exothermic recombination reactions.

4) Peak heat flux and temperature decay significantly at positions away from the centerline, with the maximum always occurring at the centerline of the plasma jet.

5) The use of TE capillary yields the largest stagnation pressures, possibly due to a large density of the plasma.

The present study deals with the radiative heat transfer from plasma produced by relatively low charging voltage. Future studies will consider other geometries, higher charging voltages, different window materials, as well as other heat transfer mechanisms.

Acknowledgment

This work was supported by the U.S. Army Research Laboratory and the U.S. Army Research Office under Contract DAAD19-03-1-0340 with the management of David M. Mann.

References

[1]Beyer, R. A., and Pesce-Rodriguez, R. A., "Experiments to Define Plasma–Propellant Interactions," *IEEE Transactions on Magnetics*, Vol. 39, No. 1, 2003, pp. 207–211.

[2]Fifer, R. A., Sagan, E. S., and Beyer, R. A., "Chemical Effects in Plasma Ignition," *IEEE Transactions on Magnetics*, Vol. 39, No. 1, 2003, pp. 218–222.

[3]Perelmutter, L., Sudai, M., Goldenberg, C., Kimhe, D., Zeevi, Z., Arie, S., Melnik, M., and Melnik, D., "Temperature Compensation by Controlled Ignition Power in SPETC Guns," *Proceedings of the 16th International Symposium on Ballistics*, National Defense Industrial Association, Arlington, VA, Vol. 1, 1996, pp. 145–152.

[4]Edwards, C. M., Bourham, M. A., and Gilligan, J. G., "Experimental Studies of the Plasma-Propellant Interface for Electrothermal–Chemical Launchers," *IEEE Transactions on Magnetics*, Vol. 31, No. 1, 1995, pp. 404–409.

[5]Birk, A., Del Guercio, M., Kinkennon, A., Kooker, D. E., and Kaste, P., "Interrupted-Burning Tests of Plasma Ignited JA2 and M30 Grains in a Closed Chamber," *Propellants, Explosives, Pyrotechnics*, Vol. 25, No. 3, 2000, pp. 133–142.

[6]Kim, J. U., Clemens, N. T., and Varghese, P. L., "Experimental Study of the Transient Underexpanded Jet Generated by Electrothermal Capillary Plasma," *Journal of Propulsion and Power*, Vol. 18, No. 6, 2002, pp. 1153–1160.

[7]Kappen, K., and Beyer, R. A., "Progress in Understanding Plasma–Propellant Interaction," *Propellants, Explosives, Pyrotechnics*, Vol. 28, No. 1, 2003, pp. 32–36.

[8]Li, J.-Q., Litzinger, T. A., and Thynell, S. T., "Interactions of Capillary Plasma with Double-Base and Composite Propellants," *Journal of Propulsion and Power*, Vol. 20, No. 4, 2004, pp. 675–683.

[9]Li, J.-Q., Litzinger, T. A., and Thynell, S. T., "Plasma Ignition and Combustion of JA2 Propellant," *Journal of Propulsion and Power*, Vol. 21, No. 1, 2005, pp. 44–53.

[10]Das, M., Thynell, S. T., Li, J.-Q, and Litzinger, T. A., "Transient Radiative Heat Transfer from a Plasma Produced by a Capillary Discharge," *Journal of Thermophysics and Heat Transfer*, Vol. 19, No. 4, 2005, pp. 572–580.

[11]Beyer, R. A., and Pesce-Rodriguez, R. A., "The Response of Propellants to Plasma Radiation," *IEEE Transactions on Magnetics*, Vol. 41, No. 1, 2005, pp. 344–349.

[12]Schroeder, M. A., Beyer, R. A., and Pesce-Rodriguez, R. A., "Scanning Electron Microscope Examination of JA2 Propellant Samples Exposed to Plasma Radiation," *IEEE Transactions on Magnetics*, Vol. 41, No. 1, 2005, pp. 350–354.

[13]Wren, G. P., Oberle, W. F., and Hosangadi, A., "Influence of Radiation on Grain Heating in ETC Closed Chambers," *IEEE Transactions on Magnetics*, Vol. 35, No. 1, 1999, pp. 234–239.

[14]Taylor, M. J., "Evidence for the Hypothesis of Ignition of Propellants by Metallic Vapour Deposition," *Propellants, Explosives, Pyrotechnics*, Vol. 27, No. 6, 2002, pp. 327–335.

[15]Taylor, M. J., "Ignition of Propellant by Metallic Vapour Deposition for an ETC Gun System," *Propellants, Explosives, Pyrotechnics*, Vol. 26, No. 3, 2001, pp. 137–143.

[16]Taylor, M. J., "Measurement of the Properties of Plasma from ETC Capillary Plasma Generators," *IEEE Transactions on Magnetics*, Vol. 37, No. 1, 2001, pp. 194–198.

[17]Taylor, M. J., "Spectral Acquisition and Calibration Techniques for the Measurements of Radiative Flux Incident upon Propellant," *Propellants, Explosives, Pyrotechnics*, Vol. 28, No. 3, 2003, pp. 18–25.

[18]Taylor, M. J., "Direct Measurement of Radiative Flux Incident Upon Propellant During Plasma Propellant Interactions," *Propellants, Explosives, Pyrotechnics*, Vol. 28, No. 3, 2003, pp. 26–31.

[19]Ryan, M. D., Clemens, N. T., and Varghese, P. L., "Measurements of Electrothermal–Plasma Ignition of Solid Propellants," AIAA Paper 2004-0388 Jan. 2004.

[20]Williams, A. W., and White, K. J., "Plasma–Propellant Interaction Studies: Measurements of Heat Flux Produced by Hydrocarbon Ablation-Supported Plasmas," *IEEE Transactions on Magnetics*, Vol. 37, No. 1, 2001, pp. 203–206.

[21]White, K., Williams, A. W., and Nusca, M., "Plasma Output and Propellant Radiation Absorption Characteristics," *Proceedings of 35th JANNAF Combustion Meeting*, CPIA Publ. 680, Vol. 1, Chemical Propulsion Information Analysis Center, Baltimore, MD, 1998, pp. 237–246.

[22]Williams, A. W., and Beyer, R. A., "Heat Flux Measurements of Plasmas," 39th JANNAF Combustion Meeting, Paper 2003-03990AG, June 2005.

[23]Gruber, K., Kappen, K., Voronov, A., and Haak, H., "Radiation Absorption of Propellant Gas," *IEEE Transactions on Magnetics*, Vol. 37, No. 1, 2001, pp. 161–164.

[24]Kappen, K., and Bauder, U. H., "Calculation of Plasma Radiation Transport for Description of Propellant Ignition and Simulation of Interior Ballistics in ETC Guns," *IEEE Transactions on Magnetics*, Vol. 37, No. 1, 2001, pp. 169–172.

[25]Kappen, K., and Bauder, U. H., "Simulation of Plasma Radiation in Electrothermal–Chemical Accelerators," *IEEE Transactions on Magnetics*, Vol. 35, No. 1, 1999, pp. 192–196.

[26]Ozisik, M. N., *Heat Conduction*, 2nd ed., Wiley, New York, 1993, Chap. 14.

[27]Kurabayashi, K., Asheghi, M., Touzelbaev, M., and Goodson, K. E., "Measurement of the Thermal Conductivity Anisotropy in Polyimide Films," *Journal of Microelectromechanical Systems*, Vol. 8, No. 2, 1999, pp. 180–191.

[28]Lide, D. R., (ed.), *CRC Handbook of Chemistry and Physics*, CRC Press, Boca Raton, FL, 1997, Chap. 4.

[29]Modest, M. F., *Radiative Heat Transfer*, 2nd ed., Academic Press, San Diego, CA, 2003, Chap. 2-3.

[30]Conesa, J. A., and Font, R., "Polytetrafluoroethylene Decomposition in Air and Nitrogen," *Polymer Engineering and Science*, Vol. 41, No. 12, 2001, pp. 2137–2147.

[31]Ksiazczak, A., Boniuk, H., and Cudzilo, S., "Thermal Decomposition of PTFE in the Presence of Silicon, Calcium Silicide, Ferrosilicon and Iron," *Journal of Thermal Analysis and Calorimetry*, Vol. 74, No. 2, 2003, pp. 569–574.

[32]Lewis, E. E., and Naylor, M. A., "Pyrolysis of Polytetrafluoroethylene," *Journal of the American Chemical Society*, Vol. 69, No. 8, 1947, pp. 1968–1970.

[33]Huczko, A., Lange, H., Chojecki, G., Cudziło, S., Zhu, Y. Q., Kroto, H. W., and Walton, D. R. M., "Synthesis of Novel Nanostructures by Metal–Polytetrafluoroethene Thermolysis," *Journal of Physical Chemistry B*, Vol. 107, No. 11, 2003, pp. 2519–2524.

[34]Koch, E.-C., "Review on Pyrotechnic Aerial Infrared Decoys," *Propellants, Explosives, Pyrotechnics*, Vol. 26, No. 1, 2001, pp. 3–11.

[35]Keidar, M., Boyd, I. O., and Beilis, I. I., "Model of Particulate Interaction with Plasma in a Teflon Pulsed Plasma Thruster," *Journal of Propulsion and Power*, Vol. 17, No. 1, 2001, pp. 125–131.

[36]Conesa, J. A., Marcilla, A., Font, R., and Caballero, J. A., "Thermogravimetric Studies on the Thermal Decomposition of Polyethylene," *Journal of Analytical and Applied Pyrolysis*, Vol. 36, No. 1, 1996, pp. 1–15.

[37]Wall, L. A., Madorsky, S. L., Brown, D. W., Straus, S., and Simha, R., "The Depolymerization of Polymethylene and Polyethylene," *Journal of the American Chemical Society*, Vol. 76, No. 13, 1954, pp. 3430–3437.

[38]Onu, P., Vasile, C., Ciocilteu, S., Iojoiu, E., and Darie, H., "Thermal and Catalytic Decomposition of Polyethylene and Polypropylene," *Journal of Analytical and Applied Pyrolysis*, Vol. 49, No. 1-2, 1999, pp. 145–153.

[39]Li, X.-G., and Huang, M.-R, "Thermal Degradation of Bisphenol A polycarbonate by High-Resolution Thermogravimetry," *Polymer International*, Vol. 48, No. 5, 1999, pp. 387–391.

[40]Puglisi, C., Sturiale, L., and Montaudo, G., "Thermal Decomposition Processes in Aromatic Polycarbonates Investigated by Mass Spectrometry," *Macromolecules*, Vol. 32, No. 7, 1999, pp. 2194–2203.

[41]Borucki, W. J., "Spectrographic Observations of Polycarbonate, Polyethylene, and Polyformaldehyde in Ballistic Range, Arcjet, and Diffusion Flame," *AIAA Journal*, Vol. 5, No. 7, 1967, pp. 1329–1336.

[42]Kohel, J. M., Su, L. K., Clemens, N. T., and Varghese, P. L., "Emission Spectroscopic Measurements and Analysis of a Pulsed Plasma jet," *IEEE Transactions on Magnetics*, Vol. 35, No. 1, 1999, pp. 201–204.

[43]Beyer, R. A., and Bunte, S. W., "Spatial and Temporal Temperature Studies of Electrothermal Chemical (ETC) Plasmas," Rept., BRL-TR-3324, AD-A248541, 1992; URL: www.ntis.gov [cited March 1992].

[44]Johnson, R. C., and Asundi, R. K., "A New Band System of Carbon Monoxide ($3\ ^1S \rightarrow 2\ ^1P$), with Remarks on the Ångström Band System," *Proceedings of the Royal Society of London, Series A: Mathematical and Physical Sciences*, Vol. 123, No. 792, 1929, pp. 560–574.

[45]Taylor, M. J., "A Description of the Wire Explosion Process for ETC Plasma Generators," *IEEE Transactions on Magnetics*, Vol. 39, No. 1, 2003, pp. 269–274.

[46]Taylor, M. J., "Formation of Plasma Around Wire Fragments Created by Electrically Exploded Copper Wire," *Journal of Physics D: Applied Physics*, Vol. 35, No. 1, 2002, pp. 707–709.

[47]Sueda, T., Katsuki, S., and Akiyama, H., "Early Phenomena of Capillary Discharges for an Electrothermal Gun," *Applied Physics Letter*, Vol. 68, No. 13, 1996, pp. 1766–1768.

[48]Martin, W. C., Fuhr, J. R., Kelleher, D. E., Musgrove, A., Sugar, J., Wiese, W. L., Mohr, P. J., and Olsen, K. (1999), *NIST Atomic Spectra Database* (version 2.0). National Institute of Standards and Technology, Gaithersburg, MD, http://physics.nist.gov/asd2; [cited 3 May 2006].

[49]Nusca, M. J., McQuaid, M. J., and Anderson, W. R., "Numerical Model of the Plasma Jet Generated by an Electrothermal–Chemical Igniter," *Journal of Thermophysics and Heat Transfer*, Vol. 16, No. 1, 2002, pp. 157–160.